Published in final edited form as:
J Neurosci. 2011 April 13; 31(15): 5682–5692. doi:10.1523/JNEUROSCI.5453-10.2011.

Recovery from short-term depression and facilitation is ultrafast and Ca^{2+}-dependent at auditory hair cell synapses

Soyoun Cho, **Geng-Lin Li**, and **Henrique von Gersdorff**
The Vollum Institute, Oregon Health & Science University, 3181 SW Sam Jackson Park Road, Portland, OR 97239

Abstract

Short-term facilitation and depression coexist at many CNS synapses. Facilitation, however, has not been fully characterized at hair cell synapses. Using paired recordings and membrane capacitance measurements we find that paired-pulse plasticity at an adult frog auditory hair cell synapse depends on pulse duration and inter-pulse intervals. For short 20 ms depolarizing pulses, and inter-pulse intervals between 15 to 50 ms, facilitation occurred when hair cells were held at −90 mV. However, hair cells held at −60 mV displayed only paired-pulse depression. Facilitation was dependent on residual free Ca^{2+} levels because it was greatly reduced by the Ca^{2+} buffers EGTA and BAPTA. Furthermore, low external Ca^{2+} augmented facilitation, whereas depression was augmented by high external Ca^{2+}, consistent with depletion of a small pool of fast releasing synaptic vesicles. Recovery from depression had a double-exponential time course with a fast component that may reflect the rapid replenishment of a depleted vesicle pool. We suggest that hair cells held at more depolarized *in vivo*-like resting membrane potentials have a tonic influx of Ca^{2+}; they are thus in a dynamic state of continuous vesicle release, pool depletion and replenishment. Further Ca^{2+} influx during paired-pulse stimuli then leads to depression. However, at membrane potentials of −90 mV ongoing release and pool depletion are minimized, so facilitation is revealed at time intervals when rapid vesicle pool replenishment occurs. Finally, we propose that vesicle pool replenishment kinetics is not rate-limited by vesicle endocytosis, which is too slow to influence the rapid pool replenishment process.

Keywords

auditory afferent fibers; paired-pulse depression; paired-pulse facilitation; short-term plasticity; membrane capacitance; excitatory postsynaptic current

Introduction

Auditory hair cell synapses have some distinctive features that set them apart from conventional synapses. Instead of being triggered by all-or-none action potential spikes, glutamate is continuously released with remarkable temporal precision by graded membrane potential changes in hair cells. The amplitude, duration, and frequency of sound are thus encoded by the patterns of glutamate-evoked spikes in the afferent fiber. Hair cells also have unique electron-dense disc-like structures, called synaptic ribbons, where exocytosis occurs preferentially (Zenisek et al., 2003). Although the functions of synaptic ribbons at hair cells are not completely understood, they may promote a highly synchronous form of multivesicular release (Glowatzki and Fuchs, 2002).

Correspondence should be addressed to Henrique von Gersdorff, The Vollum Institute, Oregon Health & Science University, 3181 SW Sam Jackson Park Road, Portland, OR 97239, USA. vongersd@ohsu.edu.

Short-term plasticity of hair cell synapses can be critical for auditory function. Ongoing facilitation may enhance the accuracy of signal onset with minimum delay, while short-term depression may help to match the stimuli strength for limited dynamic ranges of spiking, a process known as adaptation (Chimento and Schreiner 1991; Spassova et al., 2004). The mechanisms that underlie paired-pulse facilitation and depression vary at different synapses, and the observed behavior is a mix of the offsetting strengths of these influences. In general, at synapses with a high probability of release, depression dominates, while synapses with a low release probability tend to show facilitation (Thomson, 2000). It has been widely accepted that residual calcium from previous stimuli causes activity-dependent facilitation (Katz and Miledi, 1968), although another possible mechanism is saturation of local calcium buffers during the stimulus in a pair of stimuli (Klingauf and Neher, 1997). In contrast, depletion of a readily releasable pool of vesicles can cause synaptic depression (von Gersdorff and Matthews, 1997). In addition, postsynaptic receptors can be desensitized or saturated by repetitive exposure to neurotransmitter release (Trussell et al., 1993).

Previous studies of short-term plasticity using ribbon-type synapses generally showed only short-term depression, though experimental conditions such as intensity of stimulus, concentrations of external calcium, and internal calcium buffer varied greatly (reviewed by Edmonds, et al., 2004, and Rabl et al., 2006). The recovery rate of depression was generally fast with short and/or weak stimulus, and it was slower as the stimulus became longer and/or stronger. However, facilitation has not been so evident at ribbon-type synapses perhaps because it is masked by the strong synaptic depression.

Here we use the amphibian papilla of adult bullfrogs (*Rana catesbeiana*) to study short-term plasticity at mature hair cell synapses (Keen and Hudspeth, 2006; Li et al., 2009). At this preparation both the presynaptic hair cells and connecting postsynaptic afferent fibers are exposed and simultaneous patch-clamp recordings are possible. Our results show that hair cell synapses can show both paired-pulse depression and facilitation depending on the durations of the depolarizing pulse and/or inter-pulse intervals and on the hair cell holding potential. Furthermore, we propose that the phenomena of recovery from forward masking observed with *in vivo* fast-adapting frog afferent fiber recordings can be explained by the hair cell's recovery rate from paired-pulse depression (Megela and Capranica, 1982; Smotherman and Narins, 2000).

Materials and Methods

Hair cell preparation

Following an OHSU (IACUC) approved animal care protocol, amphibian papillae were carefully dissected from adult female or male bullfrogs (*Rana catesbeiana*) that had been sedated in ice water bath, double-pithed and decapitated. Amphibian papillae were placed in a recording chamber with oxygenated artificial perilymph containing (in mM): 95 NaCl, 2 KCl, 2 $CaCl_2$, 1 $MgCl_2$, 25 $NaHCO_3$, 3 Glucose, 1 creatine, 1 Na-pyruvate, pH adjusted to 7.30 with NaOH, and continuously bubbled with 95% O_2 and 5% CO_2 (230 mOsm). Semi-intact preparations of hair cells and their connecting afferent fibers were obtained as described by Keen and Hudspeth (2006) and Li et al. (2009). During the recordings, the preparation was perfused continuously (2–3 ml/min) with oxygenated artificial perilymph.

Electrophysiology

For whole-cell recordings, patch pipettes of borosilicate glass were pulled to resistances of 5 to 6 MΩ for hair cells and 7 to 10 MΩ for afferent fibers. Unless described otherwise, pipettes were filled with the internal solution contained (in mM): 77 Cs-gluconate, 20 CsCl, 1 $MgCl_2$, 10 TEA-Cl, 10 HEPES, 2 EGTA, 3 Mg-ATP, 1 Na-GTP and 5 Na_2-

phosphocreatine (adjusted to pH 7.3 with CsOH). Perforated patch recordings were made with nystatin (250 μg/ml, 0.4% DMSO). Patch-clamp recordings were performed with a double EPC-9/2 (HEKA Elektronik, Lambrecht/Pfalz, Germany) patch-clamp amplifier and Pulse software (HEKA) at room temperature. Hair cells and connecting afferent fibers were viewed with differential-interference-contrast microscopy through a 60x water-immersion objective lens (Olympus) and CCD camera (C79; Hamamatsu, Tokyo, Japan).

Hair cells were held at a resting membrane potential of either −60 mV or −90 mV and afferent fibers were held at −90 mV. Membrane potentials were corrected for a liquid junction potential of 10 mV. The averaged uncompensated series resistances (R_s) in whole-cell recordings were 12.6 ± 0.3 MΩ for 30 hair-cell recordings and 29.5 ± 1.3 MΩ for 25 afferent-fiber recordings. R_s was compensated in some afferent fiber recordings by up to 60% (n=10), however we did not use electronic series resistance compensation for most of the recordings because this added noise to the recordings and often resulted in the loss of the fiber recording. Therefore, an off-line R_s compensation procedure was performed for peak EPSC values following the methods outlined by Traynelis (1998) and Leão et al (2005). Each peak current was scaled by a factor K that corrects for the loss of driving force due to series resistance errors. The factor $K = (V_c - V_{rev})/(V_c - I \cdot R_s - V_{rev})$, where V_c is the command potential, V_{rev} is the calculated reversal potential (V_{rev} =0 for AMPA receptor mediated EPSCs), and I is the current at any point in time and R_s is the uncompensated series resistance. As expected (see Leão et al., 2005), the average recovery time constants of peak EPSCs from synaptic depression tended to be slightly slower after this off-line R_s compensation procedure, but this difference was not statistically significant (data not shown). The average EPSC recovery time course data shown here were thus corrected for any artificial speeding-up of the time constants due to series resistance errors. The current signal was low-pass filtered at 2 kHz and sampled at 10 μs intervals.

Capacitance Measurements

The measurements of the whole-cell membrane capacitance (C_m) from hair cells were performed under voltage-clamp with the “Sine + DC” method (Lindau and Neher, 1988; Gillis, 2000) using a double EPC-9/2 (HEKA Elektronik, Lambrecht/Pfalz, Germany) patch-clamp amplifier and Pulse software (HEKA). Patch pipettes were coated with dental wax to minimize their stray capacitance and to achieve better C-fast compensation. Sine waves (50 mV peak-to-peak, 1 kHz) were superposed on the holding potential, −90 mV, and the resulting current response was used to calculate C_m via a Pulse software emulator of a lock-in amplifier (Gillis, 2000). The increase of C_m (ΔC_m), evoked by membrane depolarization, was measured as $\Delta C_m = C_{m\,(response)} - C_{m\,(baseline)}$ and was used as a measure of synaptic vesicle exocytosis from hair cells. An average of $C_{m\,(response)}$ and $C_{m\,(baseline)}$ was obtained by averaging capacitance data points before and after the depolarizing pulse, and the amount of points used depended on the interpulse interval for paired pulses.

Data Analysis

Data analysis was performed with Igor Pro software (Wavemetrics, Lake Oswego, OR) and Prism (GraphPad Software, San Diego, CA). Statistical significance was assessed with paired and unpaired Student’s *t* tests with $p < 0.05$ considered significant. Data are expressed as mean ± SEM.

Results

Short-term plasticity at hair cell synapses

We studied short-term plasticity using a pair of pulses in adult auditory hair cell synapses from the bullfrog amphibian papilla. Hair cells were stimulated by a pair of 20 ms

depolarizing pulses from a holding potential of −60 mV to −30 mV with various inter-pulse intervals (from 3 ms to 500 ms) and EPSCs were recorded from the connected postsynaptic afferent fibers (Fig. 1). EPSCs during the depolarizing pulse consisted of a fast, transient component and a smaller sustained component. As the inter-pulse interval was made shorter, the peak amplitude of the second EPSC became smaller (Fig. 1A). With these stimulating conditions and protocols, hair cell synapses displayed severe paired-pulse depression.

Although −60 mV is closer to the physiological *in vivo* resting membrane potential of auditory hair cells (Crawford and Fettiplace, 1980; Pitchford and Ashmore, 1987), at this membrane potential significant Ca^{2+} influx and glutamate release occur (Li et al., 2009). To uncover the underlying mechanisms of short-term plasticity in the absence of this continuous Ca^{2+} influx, we also used −90 mV as a holding potential for the presynaptic hair cells. When we stimulated hair cells using a pair of 20 ms pulses from −90 mV to −30 mV with various inter-pulse intervals (from 3 ms to 500 ms), hair cell synapses showed both paired-pulse depression and facilitation depending on the inter-pulse interval (Fig. 1B). At short inter-pulse intervals, paired-pulse depression dominated and EPSCs evoked by the second pulse usually showed only a small fast peak, whereas for inter-pulse intervals from 15 ms to 50 ms facilitation was observed (Fig. 1B). Note also that for hair cells held at −90 mV the recovery time from paired-pulse depression was greatly accelerated (Fig. 1B), a finding that may help to explain frequency selectivity of exocytosis in frog saccular hair cells, where a short hyperpolarizing gap in a depolarizing step enhances the overall amount of exocytosis (Rutherford and Roberts, 2006). Full recovery of the EPSC peak was evident at inter-pulse intervals of < 20 ms for hair cells held at −90 mV, whereas recovery was not complete for hair cells held at −60 mV even after inter-pulse intervals of 200 ms (Fig. 1A and 1B).

We next calculated the paired-pulse ratio ($EPSC_2/EPSC_1$) from the peak amplitude of EPSCs. For hair cells held at −60 mV, at a 3 ms inter-pulse interval the averaged paired-pulse EPSC peak ratio was 0.23 ± 0.09 (n = 9), whereas for hair cells held at −90 mV this averaged paired-pulse EPSC peak ratio was 0.45 ± 0.06 (n = 7) (Fig. 2A and 2B). EPSC peaks thus undergo more severe depression at very short inter-pulse intervals when hair cells are held at −60 mV. As the inter-pulse interval became longer, the paired-pulse ratio recovered and for a certain range of inter-pulse intervals, such as 20 ms or 50 ms, the peak amplitude of the second EPSC became even bigger than the first EPSC peak amplitude for hair cells held at −90 mV (Fig. 2B). With a 20 ms inter-pulse interval, the averaged paired-pulse ratio was 1.26 ± 0.05 (n = 8) and with a 50 ms inter-pulse interval, the averaged paired-pulse ratio was 1.37 ± 0.06 (n = 8) (Fig. 2B). Paired-pulse facilitation dwindled as the inter-pulse interval became even longer and the averaged paired-pulse ratio eventually approached 1 (Fig. 2B). The recovery of peak EPSC paired-pulse depression for hair cells held at −60 mV could be fit with a double exponential function with fast (τ_f = 15.0 ms; 64 %)and slow (τ_s = 581 ms; 36 %) time constants, which produces a median time constant τ_{median} = 213 ms (Fig. 2A). For hair cells held at −90 mV, the averaged paired-pulse ratio with inter-pulse interval from 3 ms (paired-pulse ratio 0.45 ± 0.06) to 50 ms (paired-pulse ratio 1.37 ± 0.06) increased as a single exponential function with 10.9 ms time constant (Fig. 2B).

We also checked whether Ca^{2+} influx through the L-type calcium channels on hair cells contributed to paired-pulse depression and facilitation. We calculated Ca^{2+} charge (Q_{Ca}) by integrating Ca^{2+} currents evoked by a pair of pulses. Both at −60 mV and −90 mV, the ratio of second and first Q_{Ca} (Q_{Ca2}/Q_{Ca1}) was consistently very close to 1 regardless of paired-pulse depression or facilitation (Fig. 2A and 2B). This indicates that Ca^{2+} current inactivation or facilitation does not contribute significantly to paired-pulse plasticity at hair cell synapses.

We next compared the paired-pulse ratios for hair cells held at −60 mV and at −90 mV (Fig. 2C). When we held hair cells at −90 mV, hair cell synapses showed first paired-pulse depression for very short intervals, a brief overshoot period of paired-pulse facilitation, and eventually a recovery back to 1 within about 100 ms. In contrast, paired-pulse depression generally dominated for all ranges of the inter-pulse intervals when hair cells were held at −60 mV (Fig. 2A and 2C). Furthermore, hair cells held at −60 mV showed a significantly stronger initial paired-pulse depression for short intervals, such as 3 ms or 5 ms, than for hair cells held at −90 mV, and the recovery rate of paired-pulse depression was faster at −90 mV than at −60 mV (Fig. 2C). When we also calculated the paired-pulse ratio from EPSC charge transfers, the paired-pulse ratios for hair cells held at −60 mV and at −90 mV showed similar results as those obtained from EPSC peaks (Fig. 2D). Although the paired-pulse depression of EPSC charges for short intervals was less severe in comparison with that of EPSC peaks, this small difference in paired-pulse ratios from EPSC peaks and EPSC charges was not statistically significant for the individual inter-pulse intervals for hair cells held at −60 mV and at −90 mV. We also compared the peak amplitudes of the first EPSCs for hair cells held at −60 mV and at −90 mV (Fig. 2E). For seven paired recordings, we recorded EPSCs from the same synapse while holding the hair cell at −90 mV or at −60 mV. When the hair cell was held at −60 mV, the averaged amplitude of the first EPSC (1562 ± 841 pA) was larger than the first EPSC amplitude of the hair cell held at −90 mV (524 ± 292 pA; n=7). Including other paired recordings where EPSCs were recorded separately while holding the hair cells at −90 mV or −60 mV, the first EPSC peak amplitude at −60 mV (2493 ± 626 pA; n = 12) was also significantly larger than the first peak EPSC at −90 mV (613 ± 206 pA; n = 20). However, the total charge transfers of the first EPSC for hair cells held at −60 mV and at −90 mV were not significantly different for 20 ms pulses. Remarkably, the average amplitude of the peak Ca^{2+} current was also not significantly different at the two holding potentials for the same hair cell: −347± 44 pA for −60 mV and −366 ± 49 pA for −90 mV ($p > 0.2$; paired *t* test; n=8).

We next compared the recovery of peak EPSC paired-pulse depression for hair cells held at −60 mV (Fig. 2A) with a previous *in vivo* study using *Rana pipiens* frogs (Megela and Capranica, 1982). In these *in vivo* studies a sequence of two tones, 10 dB above threshold and at the fiber's best frequency, were given at variable intervals (the first and second tone durations were 750 ms and 200 ms, respectively). The recovery from response decrement was then measured. Surprisingly, the *in vivo* recovery of auditory nerve fibers originating from the amphibian papilla resembled closely our recovery curve of paired-pulse depression while hair cells were held at −60 mV (Fig. 2F). Importantly, the *in vivo* data shown here were obtained from fast-adapting fibers that have a characteristic (best) frequency of about 350 – 550 Hz (Megela, 1984; Megela and Capranica, 1982), which is also the resonant frequency of our bullfrog hair cells (409.0 ± 2.2 Hz; n = 20; data not shown). Based on the correlation of Fig 2F, we propose that paired-pulse depression observed in our *in vitro* study may be physiologically relevant to *in vivo* auditory nerve recovery from adaptation (Spassova et al., 2004).

As mentioned above, changes in hair cell Ca^{2+} influx do not seem to significantly contribute to paired-pulse EPSC depression or facilitation (Fig. 2A and 2B). Though the ratios of the Ca^{2+} charges were very close to 1 at the two different holding potentials, the ratio of Ca^{2+} charges at −60 mV was slightly above 1, whereas it was slightly below 1 at −90 mV (Fig. 2A and 2B). The kinetics of the Ca^{2+} currents at different holding potentials is shown in Figure 3. Interestingly, there was a small initial outward component in the first Ca^{2+} current at −60 mV (Fig. 3A and 3B1). This was not present when hair cells were held at −90 mV (Fig. 3B2). The Ca^{2+} currents of Figure 3B1 resemble those observed in retinal bipolar cells and may reflect a pH-mediated inhibition of Ca^{2+} current due to the exocytosis of protons (Palmer et al., 2003), or this may be related with modulation via activation of protein kinase

C (Abreu et al., 2008). It is also possible that heterogeneous types of Ca^{2+} channels exist, as in frog saccular hair cells (Su et al., 1995; Rodriguez-Contreras and Yamoah 2001). The transient outward component causes the ratio of Ca^{2+} charges to be slightly above 1 at the −60 mV holding potential. By contrast, at −90 mV, the first Ca^{2+} current shows a slightly bigger peak than the second Ca^{2+} current for short inter-pulse intervals (Fig. 3B2). This probably reflects Ca^{2+}-dependent Ca^{2+} current inactivation (von Gersdorff and Matthews, 1996; Schnee and Ricci, 2003), and the fastest component of inactivation may reflect near-channel Ca^{2+} nanodomains that can rapidly reach high Ca^{2+} levels (Grant and Fuchs, 2008). However, as the inter-pulse intervals get longer, the first and the second Ca^{2+} currents become identical.

AMPA-receptor mediated EPSCs can undergo saturation and/or desensitization during a prolonged and strong presynaptic depolarization. So, in addition to EPSC recordings, we also monitored exocytosis directly from hair cells using membrane capacitance (C_m) measurements. The electrical capacitance of a cell is proportional to the cell surface area and vesicle fusion into the plasma membrane increases the cell surface area (Lindau and Neher, 1988). Presynaptic Ca^{2+} currents from hair cells were recorded and C_m measurements used a 1 kHz sine wave superimposed on the holding potential of −90 mV. This hyperpolarized membrane potential guaranteed that Ca^{2+} current was not activated during the sine wave stimulus used to measure C_m. The change in membrane capacitance (capacitance jump; ΔC_m) was used as a measure of exocytosis. We depolarized hair cells from −90 mV to −30 mV for 20 ms with 20ms, 50 ms, 100 ms, or 200 ms inter-pulse intervals (Fig. 4A – Fig. 4C). The averaged paired-pulse ratio of ΔC_m ($\Delta C_m{}^2/\Delta C_m{}^1$) evoked by a pair of 20 ms pulses with a 20 ms inter-pulse interval was 1.30 ± 0.22 (n = 14; Fig. 4A and Fig. 4C). With a 50 ms interval, $\Delta C_m{}^2/\Delta C_m{}^1$ was 1.27 ± 0.12 (n = 15; Fig. 4C). As the results of EPSCs showed (Fig. 2), hair cells with these protocols of stimulation (a pair of 20 ms pulse with 20 ms or 50 ms inter-pulse interval) showed paired-pulse facilitation (Fig. 4A and 4C). With a 100 ms interval, $\Delta C_m{}^2/\Delta C_m{}^1$ was 1.11 ± 0.15 (n = 12) and with a 200 ms interval, $\Delta C_m{}^2/\Delta C_m{}^1$ was 1.08 ± 0.09 (n = 9; Fig. 4B). As the inter-pulse interval became longer, $\Delta C_m{}^2/\Delta C_m{}^1$ approached a value of 1 (Fig. 4C), which was also consistent with the results obtained from EPSCs (Fig. 2).

To completely deplete the fast component of release (Li et al., 2009), we next used a longer duration of depolarization to stimulate the hair cells (Fig. 4D and 4F). When hair cells were depolarized from −90 mV to −30 mV for 200 ms, we also measured how fast the paired-pulse depression recovered. The averaged $\Delta C_m{}^2/\Delta C_m{}^1$ was measured with various inter-pulse intervals (20 ms, 50 ms, 100 ms, 200 ms, 500 ms, 1 s, 2 s, 5 s, 10 s, and 15 s). Paired-pulse depression recovered as a two exponential function with a fast time constant of 83.8 ms (τ_1; 44 %) and a slow time constant 2.9 s (τ_2; 56 %) (n = 4 – 17; Fig. 4E). Comparing with the recovery rate using a shorter pulse (20 ms) from EPSC data (Fig. 2), the recovery rate of paired-pulse depression with a longer pulse (200 ms) was dramatically slower. When hair cells were depolarized from −90 mV to −30 mV for 20ms, 100 ms, 200 ms and 500 ms with a constant inter-pulse interval of 500 ms, they generally showed paired-pulse depression (Fig. 4F). With a pair of 20 ms pulses, $\Delta C_m{}^2/\Delta C_m{}^1$ was 1.09 ± 0.22 (n = 8), and with a pair of 100 ms pulses,$\Delta C_m{}^2/\Delta C_m{}^1$ was 0.97 ± 0.16 (n = 11). With a pair of 200 ms pulses, $\Delta C_m{}^2/\Delta C_m{}^1$ was 0.84± 0.06 (n = 17), and with a pair of 500 ms pulses, $\Delta C_m{}^2/\Delta C_m{}^1$ was 0.80 ± 0.03 (n = 28).

From the results of both EPSCs and ΔC_m, we have shown that hair cell synapses display both paired-pulse depression and facilitation depending on the duration of stimulation and inter-pulse interval (Fig. 2 and 4). This is quite different from other ribbon-type synapses such as those found in goldfish retinal bipolar cell terminals, which show only depression

for pulses of variable durations (Mennerick and Matthews, 1996; Burrone and Lagnado, 2000; Palmer et al., 2003; Coggins and Zenisek, 2009).

Ca^{2+} dependence of short-term plasticity at hair cell synapses

To study whether paired-pulse facilitation and depression at hair cell synapses are dependent on Ca^{2+}, we held presynaptic hair cells at −90 mV and measured paired-pulse ratios of EPSCs using different conditions of presynaptic Ca^{2+} buffer in the internal solution (Fig. 5A – 5C). As in Fig. 2, EPSCs were recorded from afferent fibers while connected hair cells were depolarized by a pair of 20 ms voltage step from −90 mV to −30 mV with various inter-pulse intervals (3 ms – 500 ms) and the averaged ratios of EPSC peak amplitudes ($EPSC_2/EPSC_1$) were fitted exponentially (Fig. 5). As a control condition, 2 mM EGTA, $EPSC_2/EPSC_1$ with inter-pulse intervals from 3 ms to 50 ms increased double exponentially (τ = 10.9 ms; green in Fig. 5A, same with Fig. 2B) and $EPSC_2/EPSC_1$ with inter-pulse intervals from 50 ms to 500 ms decreased as a single exponential with time constant, τ_2 = 39.2 ms (n = 6 – 9; red in Fig. 5A). When the presynaptic calcium buffer in the pipette internal solution was changed into 2 mM BAPTA (n = 4 – 8), $EPSC_2/EPSC_1$ with 3 ms, 20 ms and 50 ms inter-pulse intervals were significantly different from those of 2 mM EGTA ($p < 0.05$) (Fig. 5B). The time constant (τ) of single exponential fitting between 3 ms and 50 ms inter-pulse intervals in 2 mM BAPTA (τ_1 = 9.8 ms; green) was similar with the time constant of 2 mM EGTA (10.9 ms in Fig. 5A). $EPSC_2/EPSC_1$ with inter-pulse intervals from 50 ms to 500 ms decreased single exponentially with a time constant, 38.3 ms (τ_2)(Fig. 5B). This was also very similar with time constant in 2 mM EGTA (39.2 ms in Fig. 5A). These results indicate that paired-pulse facilitation and depression at hair cell synapses are dependent on Ca^{2+}. Although the concentration of Ca^{2+} buffer was the same, BAPTA can bind with free Ca^{2+} ions 150-fold faster than EGTA and this difference may affect the concentration of residual Ca^{2+} and paired-pulse facilitation at this synapse. The effect of 2 mM BAPTA on paired-pulse depression with very short inter-pulse interval (3 ms) may result from the decrease in the first pulse response. Indeed, the first pulse ΔC_m decreased significantly in 2 mM BAPTA (12.3 ± 1.4 fF; n = 10) compared with 2 mM EGTA (18.2 ± 1.9 fF; n = 24).

We next tested a higher concentration (10 mM) of EGTA as a presynaptic Ca^{2+} buffer (Fig. 5C and 5D). The averaged $EPSC_2/EPSC_1$ with 50 ms inter-pulse interval was significantly decreased from that of 2 mM EGTA (n = 4 – 9; $p < 0.05$). In addition, we also tested the effect of 10 mM EGTA using the ΔC_m measurements. Using 2 mM EGTA as our control Ca^{2+} buffer, a ΔC_m was evoked by a pair of 20 ms voltage steps from −90 mV to −30 mV with inter-pulse interval of 20 ms, 50 ms, 100 ms and 200 ms with 2 mM external Ca^{2+} (black in Fig. 5D, same with Fig. 4C). When we increased the internal Ca^{2+} buffer concentration from 2 mM EGTA to 10 mM EGTA, this facilitation was blocked significantly with 50 ms inter-pulse interval ($p < 0.05$; Fig. 5D, green). This also indicates that paired-pulse facilitation is Ca^{2+} dependent. Higher concentrations of EGTA (10 mM) may block facilitation at a certain range of inter-pulse intervals by removing more of free Ca^{2+} and leaving less residual Ca^{2+}. Importantly, and in contrast with 2 mM BAPTA, 10 mM EGTA (18.1 ± 2.0 fF; n = 16) did not change the first pulse ΔC_m in comparison with 2 mM EGTA (18.2 ± 1.9 fF; n = 24) and it did not change paired-pulse depression with very short inter-pulse intervals (Fig. 5C).

Manipulating the release probability by changing the extracellular Ca^{2+} concentration can alter the form of short-term plasticity that dominates at synapses (Thomson, 2000; Johnson et al., 2005). To investigate the role of Ca^{2+} in short-term plasticity further, we altered the Ca^{2+} concentration in the external bath solution during the recordings (Fig. 6). When we increased Ca^{2+} concentration to 5 mM, paired-pulse facilitation in control, 2 mM Ca^{2+} in the bath (filled squares in Fig. 6A), changed into paired-pulse depression (open circles in Fig.

6A). With all inter-pulse intervals that we tested with 5 mM external Ca^{2+} in the bath, the paired-pulse ratio decreased significantly (n = 7 – 9). These results show that high external Ca^{2+} concentrations promote paired-pulse synaptic depression (Johnson et al., 2005; Frank et al., 2010). This may result from the increase in ΔC_m evoked by the first pulse with 5 mM external Ca^{2+} in the bath. Compared with 2 mM Ca^{2+} (18.2 ± 1.9 fF; n = 24), the first pulse ΔC_m significantly increased in 5 mM Ca^{2+} (29.3 ± 2.0 fF; n = 15; $p < 0.0001$). In contrast, paired-pulse facilitation became stronger by decreasing the concentration of external Ca^{2+} to 1 mM (open triangles in Fig. 6B). With a 50 ms inter-pulse interval, the paired-pulse ratio significantly increased (n = 5 – 9; $p < 0.001$). In the case of 20 ms inter-pulse intervals, it showed the tendency of increased facilitation, but this was not statistically significant because of biological variability. In contrast to the 5 mM external Ca^{2+} condition, 1 mM external Ca^{2+} in the bath significantly decreased the first pulse ΔC_m (5.9 ± 1.4 fF; n = 9) from that with 2 mM Ca^{2+}.

We next measured ΔC_m elicited by 20 ms pulses while changing external Ca^{2+} concentrations ($[Ca^{2+}]_o$) over the range of 0.5 mM to 5 mM to study the quantitative relationship between ΔC_m and external Ca^{2+} concentration (n = 11 – 17). When we fitted the data using the equation $\Delta C_m = A \bullet [Ca^{2+}]^n$, it showed a slightly sub-linear relationship (n = 0.78; black solid line in Fig. 6C). The data could also be approximated by a linear fit (R^2 = 0.95; black dashed line in Fig. 6C). Note that unlike mouse retinal bipolar cells, exocytosis does not saturate from 2 mM to 5 mM $[Ca^{2+}]_o$ suggesting a wide dynamic range of release for hair cells (Jarsky et al., 2010). This slightly sub-linear Ca^{2+} dependence of exocytosis is similar with previous studies using mature mammalian inner hair cells (Johnson et al., 2008), or using Ca^{2+} current peak amplitudes and EPSC charge transfers with our bullfrog hair cell preparation (Keen and Hudspeth, 2006).

The underlying mechanisms for depression

The relationship between paired-pulse EPSC ratio and inter-pulse intervals (Fig. 2) suggests that there is a very small and fast component of release, which can be recovered quickly (Moser and Beutner, 2000; Spassova et al., 2004; Rutherford and Roberts, 2006; Johnson et al., 2008; Bartoletti et al., 2010). Previous studies have shown that depletion of the vesicles within the readily releasable pool can cause synaptic depression (Betz, 1970; Glavinovic and Narahashi, 1988; von Gersdorff and Matthews, 1997; Heidelberger et al., 2005). Therefore, we investigated the kinetic components of evoked EPSCs during the hair cell depolarization. We depolarized hair cells from −90 mV to −30 mV for 20 ms and 200 ms and recorded the evoked EPSCs from the afferent fibers (Fig. 7A and 7B). The transferred EPSC charges were calculated by integrating the EPSCs. For a 20 ms pulse, the EPSC charge had a single time constant (τ = 13.3 ± 1.6 ms) in five synapses, whereas in four other synapses it showed a very fast (τ_f = 3.6 ± 1.5 ms) and a slow (τ_s = 15.9 ± 2.6 ms; 78% of total charge) component. For a 200 ms pulse, the EPSC change was fit with a double exponential equation with a fast (τ_f = 12.2 ± 1.1 ms) and a slow (τ_s = 599 ± 179 ms; 81% of total charge) component (n = 4; Fig. 7). Depletion of the fast component of transmitter release ($\tau_f \approx 12$ ms) thus likely results in our observed paired-pulse depression at hair cell synapses.

It is possible that desensitization or saturation of postsynaptic AMPA receptors contribute to paired-pulse depression. To test this possibility, we simultaneously recorded ΔC_m from the presynaptic hair cell and EPSCs from the connected afferent fiber. We compared ΔC_m and the transferred EPSC charges during that time (Fig. 8). A pair of short pulses with a short interval (a pair of 20 ms depolarizations with 20 ms inter-pulse interval; Fig. 8A), a pair of short pulses with a long interval (a pair of 20 ms depolarizations with 200 ms inter-pulse interval; Fig. 8B) and a pair of long pulses with a short interval (a pair of 200 ms depolarizations with 50 ms inter-pulse interval; Fig. 8C) were tested. In all cases, the ΔC_m and EPSC charge transfers were correlated very well. This is consistent with our previous

studies with single depolarizing pulses of variable durations (Li et al., 2009) and suggests that desensitization and/or saturation of AMPA receptors may not contribute significantly to short-term plasticity. Though blockers of AMPA receptor desensitization affected EPSC responses in young rat auditory nerve fibers (Goutman and Glowatzki, 2007), studies at other ribbon-type synapses also do not show evidence for AMPA receptor desensitization (Singer and Diamond, 2006; Wölfel et al., 2007; Pang et al., 2008).

To investigate whether AMPA receptor desensitization contributes to paired-pulse depression for very short inter-pulse intervals, we compared the ratio of ΔC_m evoked by a 40 ms single pulse to ΔC_m evoked by a 20 ms pulse from the same hair cells. We chose a 40 ms pulse (equivalent to a 20 ms pulse + 0 ms interval + 20 ms pulse), because this should show maximum EPSC desensitization, if it were present. For 5 cells, we calculated the paired-pulse ratio that was derived from ΔC_m using 40 ms and 20 ms pulses [(ΔC_m of 40 ms pulse − ΔC_m of 20 ms pulse)/ΔC_m of 20 ms pulse]. This ratio for "0 ms" inter-pulse intervals was 0.62 ± 0.07, which is very close to the paired-pulse ratio for EPSC charges for 3 ms inter-pulse intervals at −90 mV hair cell potentials (0.61 ± 0.08; Fig. 2D). Together, these results strongly suggest that short-term depression at hair cell synapses results from presynaptic mechanisms within hair cells.

Exocytosis and endocytosis coupling

What are the mechanisms that control vesicle pool replenishment and recovery from paired-pulse depression? It is possible that vesicles undergo endocytosis quickly after being released and thus constitute a main source for this replenishment. Since the decay of C_m after exocytosis can be interpreted as due to endocytosis, we monitored C_m for prolonged durations to measure the rate of endocytosis. Unfortunately, we could not observe significant endocytosis with 20 ms to 500 ms long depolarizing pulses under regular whole-cell recordings in hair cells. This suggests that our capacitance jump measurements reflect solely exocytosis without being contaminated by endocytic activity. However, previous recordings obtained with the nystatin-perforated patch method showed clear endocytosis (Parsons et al., 1994; Moser and Beutner, 2000). This suggests that small mobile intracellular molecules, that are required for endocytosis, may be dialyzed during the whole-cell recording (Hull and von Gersdorff, 2004). Alternatively, it is possible that a component of our internal solution in regular whole-cell recordings may inhibit endocytosis. Previous studies of endocytosis at hair cells have reported a C_m decay time constant τ of about 7.5 s (Moser and Beutner, 2000; Schnee et al., 2005; Rutherford and Roberts, 2006; Dulon et al., 2009). Hair cells were depolarized from −90 mV to −30 mV for 20, 100, and 500 ms under the nystatin-perforated patch clamp mode of recording. C_m increased after exocytosis and returned back to the baseline exponentially (Fig. 9A). As the duration of stimulation got longer, the rate of endocytosis became slower. The decay τ of C_m was 5.1 ± 1.3 s for a 20 ms pulse (n = 9), 13.5 ± 1.8 s for a 100 ms pulse (n = 9), and 32.6 ± 8.5 s for a 500 ms pulse (n = 6). The relationship between endocytic decay τ and ΔC_m was linear ($\Delta C_m = 0.17 \bullet \tau$, $R^2 = 0.99997$; Fig. 9B). Smaller amounts of exocytosis thus have a faster rate of endocytosis, perhaps because endocytic proteins are more abundant per fused vesicle (Renden and von Gersdorff, 2007; Smith et al., 2008). Although asynchronous release after a depolarizing pulse was usually very rare for hair cells held at −90 mV, it is possible that some asynchronous release from hair cells may interfere with the rate of endocytosis measured by the decay of C_m. However, given the 10 ms to 1 second time scale for recovery from depression (Fig. 1 and Fig. 2), the endocytosis rate is relatively slow and unlikely to be rate limiting for the recovery from depression. Moreover, we could observe endocytosis routinely only in the perforated patch mode of recording. It is thus likely that vesicles recruited from reserve pools may be used preferentially to replenish the fast component of transmitter release rather than vesicles that have been freshly endocytosed. A fast clearance

rate of fused vesicular membrane after exocytosis at synaptic ribbons, that is not dependent on fast endocytosis, is also implied by these results and the rapid recovery from short-term depression (Neher and Sakaba, 2008).

Discussion

Our observations at hair cell synapses suggest that short-term facilitation was dependent on residual presynaptic Ca^{2+} levels, whereas depression resulted from the depletion of a small pool of readily releasable vesicles. An extremely rapid vesicle replenishment process allows the depleted synapse to recover quickly from depression. Finally, we suggest the recovery draws mainly from preformed vesicles mobilized from a reserve pool near the synaptic ribbon, rather than from the rapid reuse of vesicles freshly formed via the retrieval of vesicular membrane (endocytosis).

Comparisons with other ribbon-type synapses

Previous studies using other ribbon synapses, such as goldfish and rat retinal bipolar cells, photoreceptors of salamanders, frog saccular hair cells and cochlear inner hair cells of the mouse showed depression only (Mennerick and Matthews, 1996; Moser and Beutner, 2000; Palmer et al., 2003; Edmonds et al., 2004; Spassova et al., 2004; Singer and Diamond, 2006; Babai et al., 2010). However, we emphasize that previous studies used a variety of experimental protocol parameters such as the duration and amplitude of depolarization, the duration of inter-pulse intervals, external Ca^{2+} concentration, internal Ca^{2+} buffer, and holding potentials. So it is difficult to directly compare them with our study. Nevertheless, retinal bipolar cell terminals exhibit strong paired-pulse depression and a relatively slow double-exponential recovery from depression (τ_f = 1.03 s and τ_s = 11.8 s, Palmer et al., 2003; see also Mennerick and Matthews, 1996; Wan et al., 2008; Coggins and Zenisek, 2009). Rod bipolar cells in the rat retina also exhibited paired-pulse depression with a slow recovery (τ = 4 s; Singer and Diamond, 2006). However, acutely isolated frog saccular hair cells recover quickly from paired-pulse depression with a τ = 29 ms (Edmonds et al., 2004). Chick and cat afferent fibers also recover quickly from sound-evoked adaptation (chick: τ = 70 ms; Spassova et al., 2004; cat: τ_f = 22 ms and τ_s = 184 ms; Chimento and Schreiner, 1991). In immature mouse inner hair cells, depletion of the readily releasable pool also had a rapid and biphasic recovery (τ_f = 140 ms and τ_s = 3 s; Moser and Beutner, 2000). Compared with these previous studies, our recovery rate from paired-pulse depression was relatively fast (Fig. 2A and 2B), although depression elicited by a longer pulse showed slower recovery (Fig. 4E). We conclude that hair cell ribbon synapses recover more quickly from depression than retinal ribbon synapses. Perhaps hair-cell synaptic ribbons, and their surrounding vesicle mobilization machinery, are tailored for fast replenishment of depleted vesicle pools (Schnee et al., 2005). The fast time course of recovery from depression in hair cell synapses may thus reflect an acute requirement for speed in the processing of ongoing acoustic signals.

Short-term plasticity and the resting membrane potential of hair cells

When hair cells were held at −60 mV, a more physiological condition (Crawford and Fettiplace, 1980; Pitchford and Ashmore, 1987), hair cell synapses showed only depression. In contrast, the synapse showed both paired-pulse depression and facilitation at the holding potential of −90 mV. Holding hair cells at different membrane potentials provided us the experimental condition to dissect the mechanisms underlying both dominant plasticity (paired-pulse depression at −60 mV) and masked plasticity (paired-pulse facilitation at −90 mV), instead of observing only one type of behavior, or a competition of both. One explanation of these differing results can lie in the resting Ca^{2+} concentration of neurons at different holding potentials (Kobayashi and Tachibana, 1995). At −60 mV, the Ca^{2+} current

in hair cells is already slightly activated (Edmonds et al., 2004; Li et al., 2009), and the concentration of resting Ca^{2+} is probably higher than at −90 mV. This can affect many Ca^{2+}-dependent processes, such as vesicle priming for fusion, facilitation of release, and vesicle recruitment rates (Awatramani et al., 2005). Changes in intracellular Ca^{2+} (or stimulation frequency) can also modify the size of the readily releasable pool (Voets, 2000; Ruiz et al., 2011). In general, at synapses with a high probability of release, depression dominates, while synapses with a low release probability tend to show facilitation. Given the larger average EPSC amplitude of hair cells held at −60 mV compared to those held at −90 mV, it seems likely that release probability was larger for hair cells held at −60 mV, so their synapses exhibited mostly paired-pulse depression.

A relatively slow decay of residual Ca^{2+} is thought to cause facilitation at conventional synapses. Accordingly, we found that higher concentrations of a slow Ca^{2+} buffer (EGTA), or dialysis of a fast Ca^{2+} buffer (BAPTA), blocked facilitation in hair cells (Fig. 5). Moreover, a higher concentration of external Ca^{2+} evoked strong paired-pulse depression and increased Ca^{2+} influx, consistent with an increase in release probability (Fig. 6). In contrast, decreasing the concentration of external Ca^{2+} resulted in smaller amplitude Ca^{2+} currents and clear paired-pulse facilitation.

Ca^{2+} dependent release and vesicle recruitment

While many conventional synapses have shown a third to fourth order power-law dependence of release on Ca^{2+}, hair cell ribbon synapses show a linear or sub-linear Ca^{2+} dependence of neurotransmitter release (Johnson et al., 2005; Keen and Hudspeth, 2006; Goutman and Glowatzki, 2007). Moreover, there is a marked developmental change in the Ca^{2+} dependence of exocytosis (Johnson et al., 2005). Our Ca^{2+} dependence of exocytosis ($n = 0.78$; Fig. 6C) is in good agreement with previous studies from mature hair cells (Keen and Hudspeth, 2006; Johnson et al., 2008). Recently, otoferlin has been shown to be a Ca^{2+} sensor for exocytosis at mouse cochlea hair cells (Roux et al., 2006), although it is likely to also be involved in a Ca-dependent vesicle recruitment process (Pangrsic et al., 2010). The existence of unique Ca^{2+} sensors in hair cells may produce the near-linear Ca^{2+} dependence of transmitter release (Safieddine and Wenthold, 1999; Dulon et al., 2009; Beurg et al., 2010; Johnson et al., 2010).

Continuous release and endocytosis at hair cell synapses

Our results show that hair cells can release a small pool of vesicles at a fast rate ($\tau_{fast} \approx 12$ ms) and replenish this pool at comparably fast rates ($\tau_f = 15$ ms (64%) with $\tau_{median} = 213$ ms at −60 mV). How can the fastest component of release be replenished so quickly? Moreover, hair cell synapses can keep releasing vesicles at high rates during prolonged stimulation (Fig. 7B and 8C). What are the mechanisms that sustain vesicle mobilization for continuous release? We suggest here that high internal Ca^{2+} levels may facilitate vesicle mobilization. In addition, to avoid premature vesicle pool depletion and maintain a proper cell size, a fast rate of endocytosis seems necessary for hair cells. However, the fastest rate of endocytosis we observed was relatively slow ($\tau = 5.1$ s with 20 ms depolarizing pulses; Fig. 9), and may be too slow to participate significantly in the recovery from depression. In mouse hair cells, high internal Ca^{2+} concentrations (> 15 μM) promoted a faster component of endocytosis ($\tau = 300$ ms; Beutner et al., 2001), although we observed here that prolonged Ca^{2+} influx produced slower rates of endocytosis (Fig. 9). Nevertheless, it is expected that endocytosed vesicles will eventually join the releasable vesicle pool. Indeed, previous studies have demonstrated that vesicles labeled with horseradish peroxidase during endocytosis attached to the synaptic bodies of hair cells after a few minutes (Siegel and Brownell, 1986). Endocytosis will thus aid vesicle recycling during repetitive or prolonged stimulation on a

long-time basis, but it probably does not play an important role for the fast recovery from paired-pulse depression.

Adaptation and recovery from synaptic depression

Synaptic vesicles exist in distinct pools that show different fusion competency as demonstrated by multiple kinetic components of exocytosis (Neher and Sakaba, 2008). The charge transfer of EPSCs from afferent fibers showed that there were two distinct kinetic components: a fast rising, transient component ($\tau_{fast} \approx 12$ ms), and a slow, sustained component that did not saturate (Fig. 7B). Mouse cochlear inner hair cells also have a fast component of exocytosis, the readily releasable pool, that is depleted with a time constant $\tau = 10$ ms (Moser and Beutner, 2000). Previous studies have suggested that the depletion of this fast-releasing vesicle pool causes auditory adaptation and the replenishment of this exhausted vesicle pool mediates recovery from adaptation (Furukawa et al., 1978; Westerman and Smith, 1984; Moser and Beutner, 2000; Spassova et al., 2004).

Hair cells in frog amphibian papilla are tonotopically arranged and the average characteristic (or resonant) frequency of our hair cells was about 400 Hz. Our bullfrog hair cells are thus in the mid-frequency portion of the amphibian papilla, which shows fast adaptation of afferent fiber spikes in response to a pure tone (Feng et al., 1975; Megela, 1984; Lewis, 1986; Christensen-Dalsgaard and Jørgensen, 1996). Considering the similar time course of the *in vivo* recovery rate from forward masking and the *in vitro* recovery rate from paired pulse depression (Fig. 2F), we propose that the rapid recovery from spike adaptation at the auditory nerve may be mediated by the fast recovery of the hair cell ribbon synapse from synaptic depression.

Acknowledgments

This research was funded by an RO1 grant (DC04274) from the NIDCD to H.v.G., a Deafness Research Foundation grant and a Tartar fellowship to S.C., and a K99 research award from the NIDCD to G.-L. L.

References

Abreu BJ, Guimaraes M, Uliana L, Vigh J, von Gersdorff H, Prado MA. Guatimosim . Protein kinase C modulates synaptic vesicle acidification in a ribbon type nerve terminal in the retina. Neurochemistry International. 2008; 53:155–164. [PubMed: 18691623]

Awatramani GB, Price GD, Trussell LO. Modulation of transmitter release by presynaptic resting potential and background calcium levels. Neuron. 2005; 48:109–121. [PubMed: 16202712]

Babai N, Bartoletti TM, Thoreson WB. Calcium regulates vesicle recruitment at the cone ribbon synapse. J Neurosci. 2010; 30:15866–15877. [PubMed: 21106825]

Bartoletti TM, Babai N, Thoreson WB. Vesicle pool size at the salamander cone ribbon synapse. J Neurophysiol. 2010; 103:419–428. [PubMed: 19923246]

Betz WJ. Depression of transmitter release at the neuromuscular junction of the frog. J Physiol. 1970; 206:629–644. [PubMed: 5498509]

Beurg M, Michalski N, Safieddine S, Bouleau Y, Schneggenburger R, Chapman ER, Petit C, Dulon D. Control of exocytosis by synaptotagmin and otoferlin in auditory hair cells. J Neurosci. 2010; 30:13281–13290. [PubMed: 20926654]

Beutner D, Voets T, Neher E, Moser T. Calcium dependence of exocytosis and endocytosis at the cochlear inner hair cell afferent synapse. Neuron. 2001; 29:681–690. [PubMed: 11301027]

Burrone J, Lagnado L. Synaptic depression and the kinetics of exocytosis in retinal bipolar cells. J Neurosci. 2000; 20:568–578. [PubMed: 10632586]

Chimento TC, Schreiner CE. Adaptation and recovery from adaptation in single fiber responses of the cat auditory nerve. J Acoust Soc Am. 1991; 90:263–273. [PubMed: 1652600]

Christensen-Dalsgaard J, Jørgensen MB. One-tone suppression in the frog auditory nerve. J Acoust Soc Am. 1996; 100:451–457. [PubMed: 8675839]

Coggins M, Zenisek D. Evidence that exocytosis is driven by calcium entry through multiple calcium channels in goldfish retinal bipolar cells. J Neurophysiol. 2009; 101:2601–2619. [PubMed: 19244355]

Crawford AC, Fettiplace R. The frequency selectivity of auditory nerve fibers and hair cells in the cochlea of the turtle. J Physiol. 1980; 306:79–125. [PubMed: 7463380]

Dulon D, Safieddine S, Jones SM, Petit C. Otoferlin is critical for a highly sensitive and linear calcium-dependent exocytosis at vestibular hair cell ribbon synapses. J Neurosci. 2009; 29:10474–10487. [PubMed: 19710301]

Edmonds BW, Gregory FD, Schweizer FE. Evidence that fast exocytosis can be predominantly mediated by vesicles not docked at active zones in frog saccular hair cells. J Physiol. 2004; 560:439–450. [PubMed: 15308677]

Feng AS, Narins PM, Capranica RR. Three populations of primary auditory fibers in the bullfrog (*Rana catesbeiana*): their peripheral origins and frequency sensitivities. J Comp Physiol. 1975; 100:221–229.

Frank T, Rutherford MA, Strenzke N, Neef A, Pangrsic T, Khimich D, Fetjova A, Gundelfinger ED, Liberman MC, Harke B, Bryan KE, Lee A, Egner A, Riedel D, Moser T. Bassoon and the synaptic ribbon organize Ca^{2+} channels and vesicles to add release sites and promote refilling. Neuron. 2010; 68:724–738. [PubMed: 21092861]

Furukawa T, Hayashida Y, Matsuura S. Quantal analysis of the size of excitatory post-synaptic potentials at synapses between hair cells and afferent nerve fibres in goldfish. J Physiol. 1978; 276:211–226. [PubMed: 206683]

Gillis KD. Admittance-based measurement of membrane capacitance using the EPC-9 patch-clamp amplifier. Pflugers Arch. 2000; 439:655–664. [PubMed: 10764227]

Glavinovic MI, Narahashi T. Depression, recovery and facilitation of neuromuscular transmission during prolonged tetanic stimulation. Neuroscience. 1988; 25:271–281. [PubMed: 2839798]

Glowatzki E, Fuchs PA. Transmitter release at the hair cell ribbon synapse. Nat Neurosci. 2002; 5:147–154. [PubMed: 11802170]

Goutman JD, Glowatzki E. Time course and calcium dependence of transmitter release at a single ribbon synapse. Proc Natl Acad Sci U S A. 2007; 104:16341–16346. [PubMed: 17911259]

Grant L, Fuchs P. Calcium- and calmodulin-dependent inactivation of calcium channels in inner hair cells of the rat cochlea. J Neurophysiol. 2008; 99:2183–2193. [PubMed: 18322004]

Heidelberger R, Thoreson WB, Witkovsky P. Synaptic transmission at retinal synapses. Prog Retin Eye Res. 2005; 24:682–720. [PubMed: 16027025]

Hull C, von Gersdorff H. Fast endocytosis is inhibited by GABA-mediated chloride influx at a presynaptic terminal. Neuron. 2004; 44:469–482. [PubMed: 15504327]

Jarsky T, Tian M, Singer JH. Nanodomain control of exocytosis is responsible for the signaling capability of a retinal ribbon synapse. J Neurosci. 2010; 30:11885–11895. [PubMed: 20826653]

Johnson SL, Marcotti W, Kros CJ. Increase in efficiency and reduction in Ca^{2+} dependence of exocytosis during development of mouse inner hair cells. J Physiol. 2005; 563:177–191. [PubMed: 15613377]

Johnson SL, Forge A, Knipper M, Munkner S, Marcotti W. Tonotopic variation in the calcium dependence of neurotransmitter release and vesicle pool replenishment at mammalian auditory ribbon synapses. J Neurosci. 2008; 28:7670–7678. [PubMed: 18650343]

Johnson SL, Franz C, Kuhn S, Furness DN, Ruttiger L, Munkner S, Rivolta MN, Seward EP, Herschman HR, Engel J, Knipper M, Marcotti W. Synaptotagmin IV determines the linear Ca^{2+} dependence of vesicle fusion at auditory ribbon synapses. Nat Neurosci. 2010; 13:45–52. [PubMed: 20010821]

Katz B, Miledi R. The role of calcium in neuromuscular facilitation. J Physiol. 1968; 195:481–92. [PubMed: 4296699]

Keen EC, Hudspeth AJ. Transfer characteristics of the hair cell's afferent synapse. Proc Natl Acad Sci U S A. 2006; 103:5537–5542. [PubMed: 16567618]

Klingauf J, Neher E. Modeling buffered Ca^{2+} diffusion near the membrane: implications for secretion in neuroendocrine cells. Biophys J. 1997; 72:674–690. [PubMed: 9017195]

Kobayashi K, Tachibana M. Ca^{2+} regulation in the presynaptic terminals of goldfish retinal bipolar cells. J Physiol. 1995; 483:79–94. [PubMed: 7539842]

Leão RM, Kushmerick C, Pinaud R, Renden R, Li GL, Taschenberger H, Spirou G, Levinson SR, von Gersdorff H. Presynaptic Na^{+} channels: locus, development, and recovery from inactivation at a high-fidelity synapse. J Neurosci. 2005; 25:3724–3738. [PubMed: 15814803]

Lewis, ER. Adaptation, suppression and tuning in amphibian acoustical fibers. In: Moore, BCJ.; Patterson, RD., editors. Auditory Frequency Selectivity. New York: Plenum; 1986. p. 129-136.

Li G, Keen E, Andor-Ardo D, Hudspeth AJ, von Gersdorff H. The unitary event underlying multiquantal EPSCs at a hair cell's ribbon synapse. J Neurosci. 2009; 29:7558–7568. [PubMed: 19515924]

Lindau M, Neher E. Patch-clamp techniques for time-resolved capacitance measurements in single cells. Pflügers Arch. 1988; 411:137–146.

Megela AL, Capranica RR. Differential patterns of physiological masking in the anuran auditory nerve. J Acoust Soc Am. 1982; 71:641–645. [PubMed: 7085968]

Megela AL. Diversity of adaptation patterns in responses of eighth nerve fibers in the bullfrog, *Rana Catesbeiana*. J Acoust Soc Am. 1984; 75:1155–1162. [PubMed: 6609943]

Mennerick S, Matthews G. Ultrafast exocytosis elicited by calcium current in synaptic terminals of retinal bipolar neurons. Neuron. 1996; 17:1241–1249. [PubMed: 8982170]

Moser T, Beutner D. Kinetics of exocytosis and endocytosis at the cochlear inner hair cell afferent synapse of the mouse. Proc Natl Acad Sci U S A. 2000; 97:883–888. [PubMed: 10639174]

Neher E, Sakaba T. Multiple roles of calcium ions in the regulation of neurotransmitter release. Neuron. 2008; 59:861–872. [PubMed: 18817727]

Palmer MJ, Hull C, Vigh J, von Gersdorff H. Synaptic cleft acidification and modulation of short-term depression by exocytosed protons in retinal bipolar cells. J Neurosci. 2003; 23:11332–11341. [PubMed: 14672997]

Pang J, Gao F, Barrow A, Jacoby RA, Wu SM. How do tonic glutamatergic synapses evade receptor desensitization? J Physiol. 2008; 586:2889–2902. [PubMed: 18420706]

Pangrsic T, Lasarow L, Reuter K, Takago H, Schwander M, Riedel D, Frank T, Tarantino LM, Bailey JS, Strenzke N, Brose N, Müller U, Reisiner E, Moser T. Hearing requires otoferlin-dependent efficient replenishment of synaptic vesicles in hair cells. Nat Neurosci. 2010; 13:869–876. [PubMed: 20562868]

Parsons TD, Lenzi D, Almers W, Roberts WM. Calcium-triggered exocytosis and endocytosis in an isolated presynaptic cell: capacitance measurements in saccular hair cells. Neuron. 1994; 13:875–883. [PubMed: 7946334]

Pitchford S, Ashmore JF. An electrical resonance in hair cells of the amphibian papilla of the frog *Rana temporaria*. Hear Res. 1987; 27:75–83. [PubMed: 3495527]

Rabl K, Cadetti L, Thoreson WB. Paired-pulse depression at photoreceptor synapses. J Neurosci. 2006; 26:2555–2563. [PubMed: 16510733]

Renden R, von Gersdorff H. Synaptic vesicle endocytosis at a CNS nerve terminal: faster kinetics at physiological temperatures and increased endocytotic capacity during maturation. J Neurophysiol. 2007; 98:3349–3359. [PubMed: 17942618]

Rodriguez-Contreras A, Yamoah EN. Direct measurement of single-channel Ca^{2+} currents in bullfrog hair cells reveals two distinct channel subtypes. J Physiol. 2001; 534.3:669–689. [PubMed: 11483699]

Roux I, Safieddine S, Nouvian R, Grati M, Simmler MC, Bahloul A, Perfettini I, Le Gall M, Rostaing P, Hamard G, Triller A, Avan P, Moser T, Petit C. Otoferlin, defective in a human deafness form, is essential for exocytosis at the auditory ribbon synapse. Cell. 2006; 127:277–289. [PubMed: 17055430]

Ruiz R, Cano R, Casañas JJ, Gaffield MA, Betz WJ, Tabares L. Active zones and the readily releasable pool of synaptic vesicles at the neuromuscular junction of the mouse. J Neurosci. 2011; 31:2000–2008. [PubMed: 21307238]

Rutherford MA, Roberts WM. Frequency selectivity of synaptic exocytosis in frog saccular hair cells. Proc Natl Acad Sci U S A. 2006; 103:2898–2903. [PubMed: 16473940]

Safieddin S, Wenthold RJ. SNARE complex at the ribbon synapses of cochlear hair cells: analysis of synaptic vesicle- and synaptic membrane-associated proteins. European J Neurosci. 1999; 11:803–812. [PubMed: 10103074]

Schnee ME, Ricci AJ. Biophysical and pharmacological characterization of voltage-gated calcium currents in turtle auditory hair cells. J Physiol. 2003; 549.3:697–717. [PubMed: 12740421]

Schnee ME, Lawton DM, Furness DM, Benke TA, Ricci AJ. Auditory hair cell-afferent fiber synapses are specialized to operate at their best frequencies. Neuron. 2005; 47:243–254. [PubMed: 16039566]

Siegel JH, Brownell WE. Synaptic and Golgi membrane recycling in cochlear hair cells. J Neurocytol. 1986; 15:311–328. [PubMed: 3746347]

Singer JH, Diamond JS. Vesicle depletion and synaptic depression at a mammalian ribbon synapse. J Neurophysiol. 2006; 95:3191–3198. [PubMed: 16452253]

Smith SM, Renden R, von Gersdorff H. Synaptic vesicle endocytosis: fast and slow modes of membrane retrieval. Trends Neurosci. 2008; 31:559–568. [PubMed: 18817990]

Smotherman MS, Narins PM. Hair cells, hearing and hopping: a field guide to hair cell physiology in the frog. J Exp Biol. 2000; 203:2237–2246. [PubMed: 10887064]

Spassova MA, Avissar M, Furman AC, Crumling MA, Saunders JC, Parsons TD. Evidence that rapid vesicle replenishment of the synaptic ribbon mediates recovery from short-term adaptation at the hair cell afferent synapse. J Assoc Res Otolaryngol. 2004; 5:376–390. [PubMed: 15675002]

Su Z, Jiang S, Gu R, Yang W. Two types of calcium channels in bullfrog saccular hair cells. Hear Res. 1995; 87:62–68. [PubMed: 8567444]

Thomson AM. Facilitation, augmentation and potentiation at central synapses. Trends Neurosci. 2000; 23:305–312. [PubMed: 10856940]

Traynelis SF. Software-based correction of single compartment series resistance errors. J Neurosci Meth. 1998; 86:25–34.

Trussell LO, Zhang S, Raman IM. Desensitization of AMPA receptors upon multiquantal neurotransmitter release. Neuron. 1993; 10:1185–1196. [PubMed: 7686382]

Voets T. Dissection of three Ca^{2+}-dependent steps leading to secretion in chromaffin cells from mouse adrenal slices. Neuron. 2000; 28:537–545. [PubMed: 11144362]

von Gersdorff H, Matthews G. Calcium-dependent inactivation of calcium current in synaptic terminals of retinal bipolar neurons. J Neurosci. 1996; 16:115–122. [PubMed: 8613777]

von Gersdorff H, Matthews G. Depletion and replenishment of vesicle pools at a ribbon-type synaptic terminal. J Neurosci. 1997; 17:1919–1927. [PubMed: 9045721]

Wan QF, Vila A, Zhou ZY, Heidelberger R. Synaptic vesicle dynamics in mouse rod bipolar cells. Vis Neurosci. 2008; 25:523–533. [PubMed: 18764958]

Westerman LA, Smith RL. Rapid and short-term adaptation in auditory nerve responses. Hear Res. 1984; 15:249–260. [PubMed: 6501113]

Wölfel M, Lou X, Schneggenburger R. A mechanism intrinsic to the vesicle fusion machinery determines fast and slow transmitter release at a large CNS synapse. J Neurosci. 2007; 27:3198–3210. [PubMed: 17376981]

Zenisek D, Davila V, Wan L, Almers W. Imaging calcium entry sites and ribbon structures in two presynaptic cells. J Neurosci. 2003; 23:2538–2548. [PubMed: 12684438]

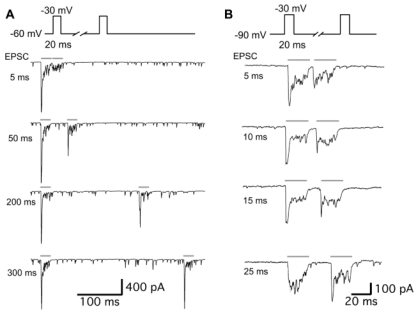

Figure 1. Paired-pulse depression and facilitation of afferent fiber EPSCs

Paired recordings of EPSCs from an afferent fiber and a connected hair cell that was depolarized by a pair of 20 ms long pulses (gray bars) from holding potentials of −60 mV (**A**) or from −90 mV (**B**) to −30 mV with various inter-pulse intervals. **A**. The stimulation protocol (top trace) and EPSCs with 5 ms, 50 ms, 200 ms and 300 ms inter-pulse intervals. The hair cell had a resting potential of −60 mV. Note the severe synaptic depression of the second EPSC for a 5 ms inter-pulse interval and the gradual recovery of the peak EPSC. **B**. The stimulation protocol (top trace) and EPSCs with 5, 10, 15, and 25 ms inter-pulse intervals. The hair cell had a resting potential of −90 mV. Note the faster recovery time course from depression of the EPSCs and the facilitation of the second peak EPSC at the 25 ms inter-pulse interval. Spontaneous EPSCs were also less frequent at a hair cell holding potential of −90 mV than at −60 mV.

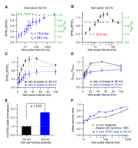

Figure 2. Recovery from paired-pulse depression and facilitation

EPSCs were recorded from the afferent fiber while a connected hair cell was depolarized by a pair of 20 ms long pulses with various inter-pulse intervals. The Ca^{2+} influx charge ratio mediated by hair-cell open Ca^{2+} channels during the pulse was calculated by integrating the Ca^{2+} currents. **A**. The paired-pulse peak EPSC ratio with hair cells held at −60 mV and inter-pulse intervals varied from 3 ms to 4 s. Data were plotted with a logarithmic scale on inter-pulse interval (n = 4 to 9 paired recordings per data point). The EPSC paired-pulse ratio recovered exponentially with fast (τ_f = 15.0 ms; 64 %) and slow (τ_s = 581 ms) time constants (the blue dashed curve shows the exponential fits). The gray dashed line indicates that the ratio is 1 ($EPSC_2 = EPSC_1$). The ratio of Ca^{2+} charge (Q_{Ca2}/Q_{Ca1}) was about 1 (0.99 – 1.05; green, right axis). **B**. The EPSC peak ratios with hair cells held at −90 mV (n = 4 – 8). The red dashed line shows a single exponential fit. From 3 ms to 50 ms intervals, the paired-pulse ratio increased exponentially (τ = 10.9 ms). Q_{Ca2}/Q_{Ca1} was relatively constant (0.96 – 0.99; green, right axis). **C**. The relationship between EPSC peak ratios and inter-pulse intervals (3 ms to 100 ms) when hair cells were held at −90 mV (n = 4 – 8) and at −60 mV (n = 5 – 9). **D.** The relationship between EPSC charge ratios and inter-pulse intervals (3 ms to 100 ms) when hair cells were held at −90 mV (n = 6) and at −60 mV (n = 4 – 6). **E.** The peak amplitudes of the first EPSCs for hair cells held at −60 mV were normalized to the first EPSCs at −90 mV. For seven paired recordings, the normalized peak of the first EPSC at −60 mV increased significantly (2.6 ± 0.8; n=7). **F.** Paired-pulse depression of hair cells held at −60 mV (blue filled square; same data as in **A**) shows similar recovery rates to that of *in vivo* fast-adapting afferent fiber spikes recovering from a pure tone sound stimulus in *Rana pipiens* frogs (black open square; modified with permission from Megela and Capranica, 1982).

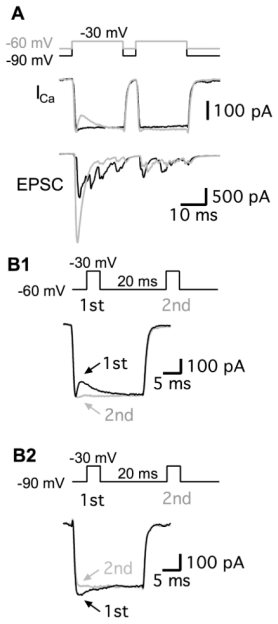

Figure 3. A comparison of Ca^{2+} currents from hair cells held at −60 mV and −90 mV

A. Hair cells were depolarized from −60 mV (gray) or −90 mV (black) to −30 mV for 20 ms with 5 ms inter-pulse intervals in the same paired recording. Ca^{2+} currents (I_{Ca}) showed similar peaks at both holding potential but the first I_{Ca} at −60 mV showed a transient outward component (or Ca^{2+} current inhibition). Note the larger first pulse EPSC amplitude when hair cells are held at −60 mV and the strong paired-pulse depression (gray trace). **B1 and B2.** Ca^{2+} currents were evoked by a pair of 20 ms pulses with a 20 ms inter-pulse interval from holding potentials of −60 mV (**B1**) or −90 mV (**B2**) to −30 mV at the same hair cell. The first Ca^{2+} currents (black) and the second Ca^{2+} currents (gray) were superimposed. At −60 mV, the first Ca^{2+} current showed a transient outward component. (**B1**). At −90 mV, the first Ca^{2+} current showed a slightly larger peak (**B2**).

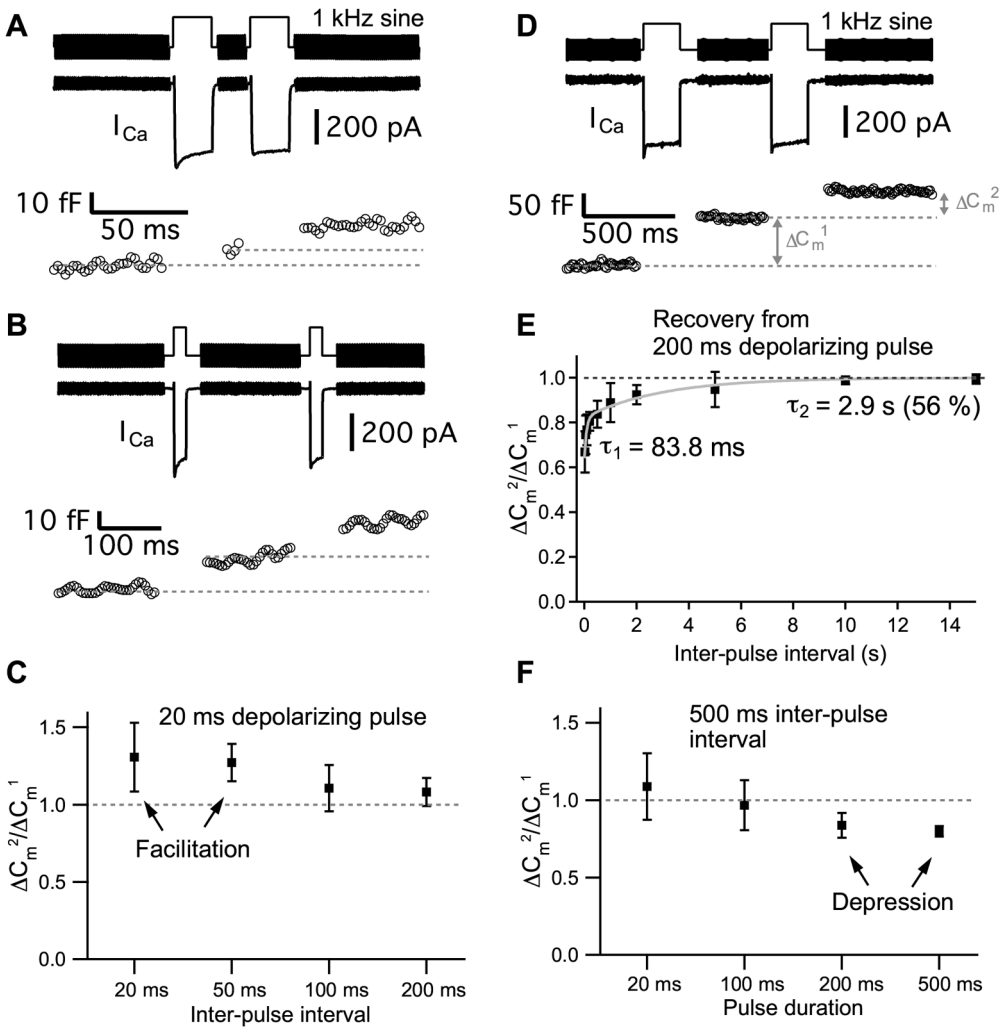

Figure 4. Paired-pulse depression and facilitation measured with membrane capacitance (C_m) changes from hair cells

Hair cells were depolarized from −90 mV to −30 mV. **A**. Calcium current (I_{Ca}) and capacitance jump (ΔC_m) evoked by a pair of 20 ms pulses with 20 ms inter-pulse interval shows paired-pulse facilitation ($\Delta C_m^2/\Delta C_m^1 > 1$). **B**. I_{Ca} and ΔC_m evoked by a pair of 20 ms pulse with 200 ms inter-pulse interval. $\Delta C_m^2/\Delta C_m^1$ was close to 1. **C**. The averaged ratio of ΔC_m ($\Delta C_m^2/\Delta C_m^1$) evoked by a pair of 20 ms voltage steps from −90 mV to −30 mV with inter-pulse interval of 20 ms, 50 ms, 100 ms and 200 ms. **D**. I_{Ca} and ΔC_m evoked by a pair of 200 ms pulses with 500 ms inter-pulse interval. **E**. Recovery from depression elicited by a pair of 200 ms pulses. The averaged $\Delta C_m^2/\Delta C_m^1$ was measured with various inter-pulse intervals (20 ms, 50 ms, 100 ms, 200 ms, 500 ms, 1 s, 2 s, 5 s, 10 s, and 15 s; n = 4 – 17). Paired-pulse depression recovered with a two exponential time course with time constants of 83.8 ms (τ_1) and 2.9 s (τ_2). **F**. ΔC_m evoked by a pair of voltage steps from −90 mV to −30 mV for various durations (20 ms, 100 ms, 200 ms and 500 ms) with 500 ms inter-pulse interval. The dashed line indicates that $\Delta C_m^2/\Delta C_m^1$ is 1.

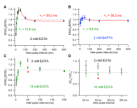

Figure 5. Ca^{2+} buffer dependence of paired-pulse ratios

EPSCs were elicited with a pair of 20 ms pulses from −90 mV to −30 mV (**A – C**). In **A** and **B**, EPSCs were recorded from afferent fibers while the hair cells were depolarized by a pair of 20 ms voltage steps from −90 mV to −30 mV with various inter-pulse intervals (3 ms – 500 ms). The averaged paired-pulse ratios of EPSC peak amplitudes ($EPSC_2/EPSC_1$) were fit by exponentials (green and red lines). In **D**, paired-pulse ratio was calculated from ΔC_m evoked by a pair of 20 ms voltage step from −90 mV to −30 mV with inter-pulse interval of 20 ms, 50 ms, 100 ms and 200 ms. **A**. The averaged $EPSC_2/EPSC_1$ with 2 mM EGTA as an internal calcium buffer in hair cells (black; n = 6 – 9). $EPSC_2/EPSC_1$ with inter-pulse intervals from 3 ms to 50 ms (3, 5, 10, 15, 20, 30 and 50 ms) increased exponentially (τ = 10.9 ms, green). The red line shows a single exponential fit with a time constant of 39.2 ms. **B**. The averaged $EPSC_2/EPSC_1$ with 2 mM BAPTA as an internal calcium buffer in hair cells (blue; n = 4 – 8). $EPSC_2/EPSC_1$ with 3 ms, 20 ms and 50 ms inter-pulse intervals were significantly different from those of 2 mM EGTA ($p < 0.05$). The time constant of a single exponential fit between the 3 ms and 50 ms intervals was 9.8 ms (τ_1; green) and the exponential time constant between 50 ms and 500 ms intervals was 38.3 ms (τ_2; red) **C**. The averaged paired-pulse ratio of EPSCs (3, 5, 10, 20, 50, 100 and 200 ms inter-pulse intervals) with 10 mM EGTA internal calcium buffer in the hair cells (green squares; n = 4 – 9). The averaged paired-pulse ratio with 10 mM EGTA was significantly decreased only for the 50 ms interval compared to 2 mM EGTA (red asterisk, $p < 0.05$). **D**. With 10 mM EGTA (green filled circle), $\Delta C_m{}^2/\Delta C_m{}^1$ was not significantly different from 2 mM EGTA (black open square, same data as in with Fig. 4C) except for the data point with 50 ms interval (red asterisk; $p < 0.05$).

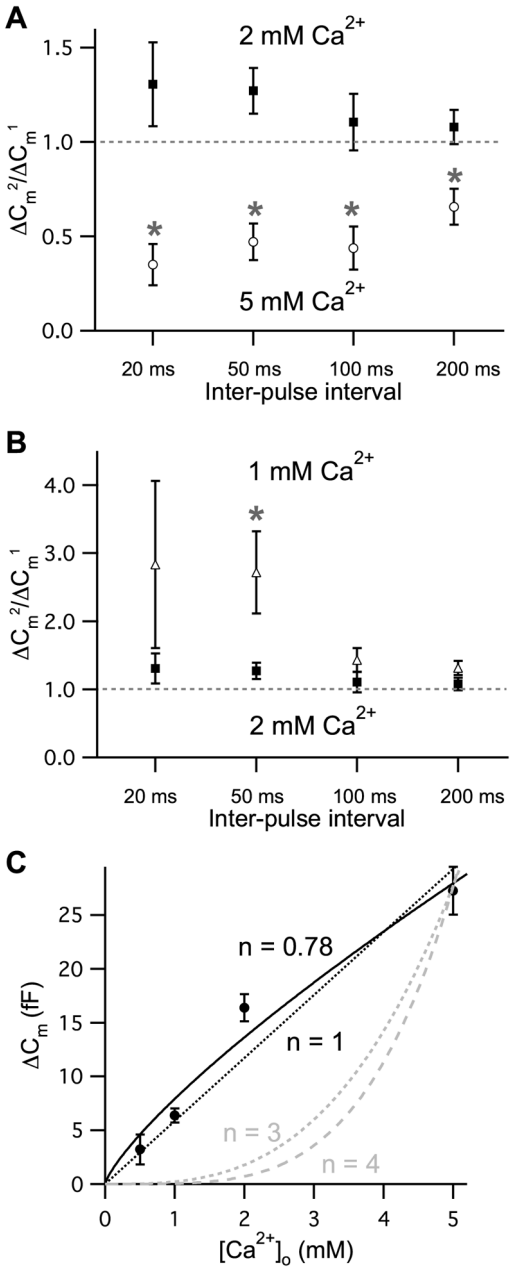

Figure 6. Dependence of paired-pulse ratios on external Ca^{2+} concentration

ΔC_m evoked by a pair of 20 ms voltage steps from −90 mV to −30 mV with inter-pulse interval of 20 ms, 50 ms, 100 ms and 200 ms with 2 mM EGTA as an internal Ca^{2+} buffer. **A**. When the external Ca^{2+} concentration was increased from 2 mM (filled squares) into 5 mM (open circles), the averaged paired-pulse ratios of ΔC_m with inter-pulse intervals ranging from 20 ms to 200 ms were significantly decreased (n = 7 – 9; asterisk; $p < 0.001$). **B**. When the external Ca^{2+} concentration decreased to 1 mM (open triangles), the averaged paired-pulse ratios of ΔC_m with inter-pulse intervals ranging from 20 ms to 200 ms were increased (n = 5 – 9) comparing with data in 2 mM external Ca^{2+} (filled squares). The ratio especially with 50 ms interval was significantly increased (asterisk; $p < 0.001$). **C**. The relationship between ΔC_m and external Ca^{2+} concentration ($[Ca^{2+}]_o$) for a 20 ms long depolarizing pulse (n = 11 – 17). The lines are fits using the equation $\Delta C_m = A \bullet [Ca^{2+}]^n$. The

best fit to the data is shown by the black solid line (n = 0.78). The gray dashed lines (n = 3 or n = 4) demonstrate the third and the fourth power relationships between $[Ca^{2+}]_o$ and ΔC_m respectively. The black dashed line is a linear fit ($R^2 = 0.95$).

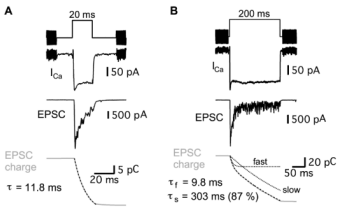

Figure 7. Prolonged hair cell depolarizations evoke EPSCs with two kinetic components

Paired recordings of hair-cell Ca^{2+} currents (I_{Ca}) and EPSCs from the connected afferent fiber. Examples of EPSCs evoked with 20 ms (**A**) and 200 ms (**B**) step depolarizations from a holding potential of −90 mV to −30 mV at the same hair cell to afferent fiber synapse. Black dashed lines are exponential fits of calculated EPSC charges (gray).With a 20 ms pulse, the exponential time constant (τ) was 11.8 ms. The EPSC charge transfer (gray) evoked by a 200 ms stimulus shows fast and slow components. The time constant of the fast component (τ_f) was 9.8 ms and the time constant of the slow component (τ_s) was 303 ms (87% of the total amplitude). The dashed black lines show the fast and slow components of the double-exponential fit to the data.

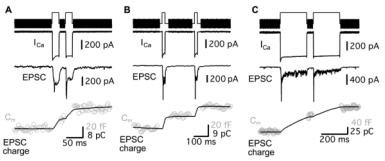

Figure 8. Paired recordings and simultaneous ΔC_m measurements

EPSCs mediated by AMPA receptors are not significantly desensitized or saturated during exocytosis with pairs of 20 ms (**A** and **B**) or 200 ms (**C**) depolarizing pulses from a holding potential of −90 mV to −30 mV in hair cell synapses. Presynaptic calcium current (I_{Ca}), membrane capacitance (C_m; gray open circle, bottom) and afferent fiber EPSC were simultaneously recorded while a voltage-clamped hair cell was depolarized by a pair of 20 ms pulses with 20 ms inter-pulse interval (**A**) or by a pair of 20 ms pulse with 200 ms inter-pulse interval (**B**) or by a pair of 200 ms pulse with 50 ms inter-pulse interval (**C**). The intermediate changes of EPSC charge transfer (black lines) are well correlated with the increases of ΔC_m (gray open circles) after the traces are normalized to the peak EPSC and ΔC_m changes.

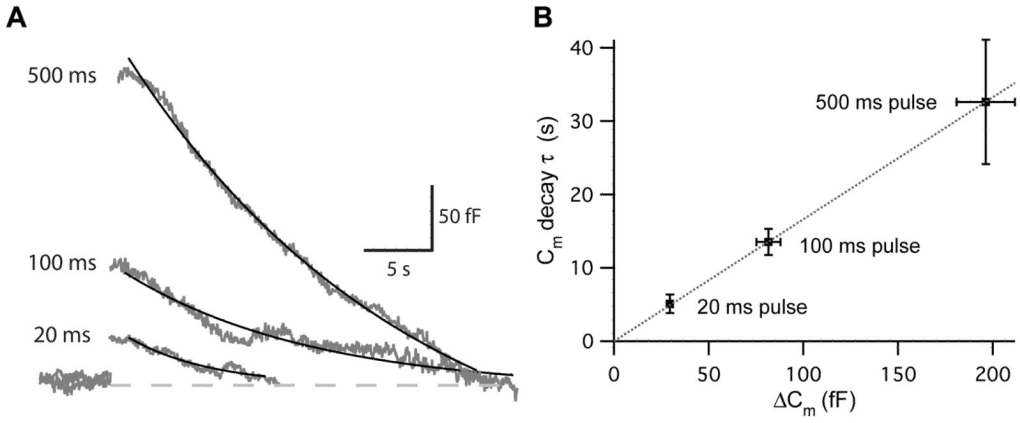

Figure 9. The coupling of exocytosis to endocytosis at hair cell synapses

The kinetics of endocytosis was measured using the nystatin-perforated patch mode of recording. **A**. C_m traces with 20 ms, 100 ms, and 500 ms long step depolarizations from −90 mV to −30 mV (gray). The decay of C_m was fit with a single exponential function (black trace). **B**. The relationship between the ΔC_m and the C_m decay time constant (τ) shows a linear relationship ($R^2 = 0.99997$). The rate of endocytosis is thus faster when the amount of exocytosis is smaller.